Environmental Science Advances

ROYAL SOCIETY OF CHEMISTRY

PAPER

View Article Online
View Journal

Cite this: DOI: 10.1039/d5va00332f

Heat and cities: using vehicle-borne sensing to capture hyperlocal spatio–temporal urban thermal complexities

Yanzhe Yin, *[a] Andrew Grundstein,[a] Deepak R. Mishra,[a] Navid Hashemi Tonekaboni, [b] Lakshmish Ramaswamy,[c] John A. Miller[c] and John Dowd[d]

Received 21st September 2025
Accepted 12th January 2026

DOI: 10.1039/d5va00332f

rsc.li/esadvances

Extreme heat events are becoming a growing concern for urban residents, with increased frequency and intensity. Understanding urban heat dynamics and thermal exposure is critical for identifying and mitigating heat hazards. Most studies of urban heat dynamics use satellite-derived or weather station data that are limited in temporal and spatial resolutions. Improving urban sustainability requires new ways to capture hyperlocal ambient air temperature (AAT) information within complex, built environments. Drive-by-sensing offers great potential in capturing the spatiotemporal dynamics of urban heat. Our paper demonstrates the broader application of temporally dense hyperlocal AAT data obtained using a novel drive-by-sensing framework. Using 2 million AAT data points collected between May–September 2019, we examine the thermal complexities of a mid-sized city, including the spatio–temporal dynamics of hotspots and areas of extreme heat exposure. This high spatiotemporal dataset reveals differing heat profiles under different weather conditions and at different times of day, with temperature variations of up to 12 °C between hot and cold spots. These hotspots move around the city and were not all found near urban cores. This drive-by-sensing approach has the potential to be scaled and used by government entities to make cities more heat resilient and sustainable.

Environmental significance

Extreme heat is increasingly affecting the life and well-being of urban residents. Although many studies have shown that extreme heat is stronger in urban areas, we do not know how transient hotspots are across the city, which may inform how communities approach heat mitigation. With millions of ambient temperature observations through a novel drive-by-sensing framework, we demonstrate new ways of collecting and analyzing hyperlocal data for citywide hotspot analysis. Our findings demonstrate the complexities of the urban thermal landscape, with hotspots varying over space-time and differences as high as 12 °C at any given time. These heterogeneous thermal patterns highlight the need to adapt a more spatially comprehensive and environmentally just mitigation strategy that considers the magnitude of heat and human exposure. And such drive-by sensing techniques and design can be implemented in various environmental monitoring studies.

1. Introduction

Extreme heat events pose an increasing threat to human health and safety[1–3] as heat waves become more prolonged, intense, and frequent under a changing climate.[4,5] The summer of 2022 was one of the hottest on record, resulting in unprecedented heat waves across the globe.[6] For instance, Western Europe faced a "heat apocalypse," and widespread fires (The Guardian, 2022); China experienced three massive heat waves that buckled roads and damaged roofs (Reuters, 2022). A heat wave in Tunisia damaged crops, led to fires, and broke a 40-year high-temperature record in the capital, Tunis (Reuters, 2022). To date, over one-third of warm season heat-related deaths can be attributed to anthropogenic climate change.[7]

Although many vulnerable populations face risks from extreme heat, urban residents are especially susceptible to heat-related health issues due to the urban heat island effect, which intensifies the warming associated with broader human-induced climate change.[8] Thus, managing urban heat is fundamental to urban resiliency in the face of climate change, as the IPCC AR6 report projects that global temperature increases will exceed 1.5 °C in the 21st century.[9] Given these projections, enhancing resiliency is a notion central to UN Sustainable Development Goals (SDGs) and the 2021 UN Climate Change Conference (COP26). Measures to reduce heat

[a]Department of Geography, University of Georgia, Athens, GA 30602, USA. E-mail: Yanzhe.Yin@uga.edu
[b]Department of Computer Science, College of Charleston, Charleston, SC 29424, USA
[c]Department of Computer Science, University of Georgia, Athens, GA 30602, USA
[d]Department of Geology, University of Georgia, Athens, GA 30602, USA

impacts include the use of water bodies, grass, plants, shading infrastructure, trees, and urban ventilation pathways, among others.[10,11] To implement these measures effectively, city planners and other stakeholders need hyperlocal information on thermal conditions that can guide the optimal use of resources for effective heat mitigation.[12,13]

Recognizing this need for detailed spatial information, new approaches to assessment and monitoring have been identified as crucial steps in the recent IPCC report for managing urban heat. Emerging technologies have also been identified as a promising pathway for monitoring and assessing thermal complexities and extreme ambient air temperature (AAT) variations within urban areas or known Urban Heat Islands (UHIs).[14] There have been a wide variety of studies using moderate resolution datasets on the distribution, structure, and dynamics in UHIs corresponding to cities.[15–17] While these moderate resolution studies have provided valuable insights into city-scale UHI patterns, they lack the spatial detail needed for neighborhood-level heat mitigation planning.

To address this limitation, advanced technologies have increasingly been used in monitoring temperature, including crowdsourcing weather data,[8,18] and high-resolution (hi-res) thermal imagery from airborne, mostly drone, or satellite sensors.[19,20] These technologies enable studying AAT with hi-res land surface temperature (LST) but still have limitations regarding spatial and temporal resolution, coverage area, and data gaps. Furthermore, LST is often not perfectly correlated with AAT,[21,22] which is a more relevant metric in heat–health relationships.[23] In recent years, various cities such as Atlanta, Birmingham, UK, and Helsinki, Finland, have developed high density *in situ* networks to capture local AATs, although cost and ability to distribute over large urban areas can be limiting factors.[24] One promising hi-res approach for monitoring hyperlocal AATs is drive-by-sensing, which uses vehicle-mounted sensors to continuously collect various types of data (*e.g.*, temperature, noise, and air quality)[25] across an urban environment. Despite its potential, we could not find any study that has focused on one testbed with multiple months of data collection to capture the daily, weekly, and monthly high-resolution ground level AAT variations. Most studies only tested for a few days or once every few years.[26] To fill this gap, in this study, we present the dynamics in urban heat hotspots using 7-month data acquired at a hyperlocal spatio–temporal scale within a mid-sized city. This paper shows the potential of temporally dense hyperlocal AAT data collected using emerging technologies such as drive-by sensing in an urban environment.

Our goal in this study is to enhance understanding of urban thermal complexities by using frequent, localized apparent air temperature data collected from a dense network of drive-by sensors in an urban setting. In particular, we aim to achieve the following objectives:

- Identify the thermal variations in urban environments by analyzing areas of hotspots and cold spots, using drive-by sensed data collected along the streets.
- Second, compare these findings with 30 m resolution satellite-derived LST products that are typically used in urban heat mapping.
- Finally, demonstrate an improved understanding of human thermal exposures by utilizing temporally dense hyperlocal AAT data, which could guide heat mitigation planning.

2. Materials and methods

We capture the thermal complexities of the urban environment using drive-by sensing data incorporated with spatial–temporal hotspot analysis. This research first visualized the collected raw data with different aggregations to better visualize spatio–temporal patterns and hotspots. Then the principal objective is to further identify if and how hotspots may vary over space and time.

2.1 Study site and drive-by sensing data collection

We conducted our study to demonstrate the utility of hyperlocal multi-temporal AAT data in a mid-sized city in the southeast USA, Athens, Georgia, near 33.95° N, 83.36° W. Athens is the center of a mid-sized metropolitan area with a population of over 200 000. It is in a humid subtropical climate zone in the southeastern US, characterized by long and hot summers transitioning into short and cold winters.[27] Average monthly temperatures range from 6.4 °C in January to 27.0 °C in July; the maximum temperature on average reaches 32 °C or higher on 58 days annually with most of these days from June to August.[28] During the study, sampling emphasized the majority of road networks in Athens-Clarke County (ACC), including Downtown Athens and the University of Georgia (UGA). Downtown Athens has the heaviest traffic in town, with many restaurants and buildings. UGA has a large population of teachers, students, and staff exceeding 50 000 and a well-vegetated landscape with tall trees and bushes distributed through campus. Athens, GA, is an ideal location for this study because it has diverse urban landscapes, experiences long, hot summers, and is of appropriate size and connectivity to encompass most of the populated areas accessible by buses carrying our sensor platform.

Having established Athens, GA, as an appropriate testbed, we deployed our mobile monitoring system across the city's public transit network. We undertook daily mobile monitoring on both city and campus buses from May 1st to December 1st, 2019, using May to September data for analysis. 40 city and campus buses were equipped with an Arduino microprocessor-operated fast-response air temperature measurement and data integration platform (SI Appendix, Fig. S6). Each platform had a core microprocessor, a timeclock, a GPS unit, a DS18B20 temperature sensor, a microSD card, wires, and a battery. The program was written in Arduino/C language and included data management, quality control, sleep and wake-up, and GPS time calibration functions, facilitating extensive, routine measurements. The air temperature sensors were fast-response (0.2 Hz) laboratory-grade DS18B20 waterproof sensors. Details about routine time calibrations and QA/QC protocols/algorithms were already published.[18] The location of the sensor was reported by the GPS unit every 5 seconds. QA data were collected every night after the buses returned to the bus terminal because the QC protocol mandated $a \pm 1$ °C accuracy.

The sensors were positioned on all active buses to optimize route coverage, where the selection and design of routes were planned by the transit offices. Buses continued to operate on weekends and holidays, but with reduced schedules and routes. During weekdays, the buses left parking lots at around 6 am local time, and we collected route data from sensors mounted on buses that traversed the Athens area until 7 pm and nighttime data for QA/QC only. The data were cleaned and filtered by excluding readings below 10 °C or above 50 °C during the summer. In total, we collected 12 million observations at 5-second intervals for the summer and fall of 2019, from which 2 million points were selected for analysis. Below is the detailed bus route map (SI Appendix, Fig. S1a) and an image of a sensor on the bus (SI Appendix, Fig. S1b). All routes consist of uniform asphalt surfaces. While acknowledging that various environmental factors could influence temperature readings, we took measures to minimize their impact by positioning the sensor in a well-ventilated area away from direct sunlight. Also, the sensor was placed approximately 0.5 m above the ground for practical purposes after consultation with our transit partners. While this is lower than traditional air temperature measurements, which are often at about 1.5 m, the turbulent mixing from the moving buses would reduce the environmental lapse rate and associated temperature differences.[29] We also wanted to ensure that the sensor was located in a spot that approximates the typical human experience near the road. Despite the possibility of heat waste and wind cooling impacts, we did not disregard their potential effects on the readings, and previous research suggests that these impacts are negligible.[30]

2.2 Data reduction

The raw dataset presented significant analytical challenges due to its volume and spatial heterogeneity. Our dataset for analysis contains 2 million data points where patterns may be challenging to identify. We aggregate the data by assigning each data point to the nearest 30-meter road segment based on its GPS coordinates. This approach enhances interpretation and aligns the resolution with Landsat 8 satellite-derived LST products for comparative analysis. This method also avoids certain overrepresenting areas within our study area, like downtown and campus centers. Basically, downtown and campus center can have more than 10 buses visits every hour which can add up to 100 data points at most, whereas suburban residential places might have only 1 bus route and 10 data points with a reduced schedule. After averaging, each road segment will be represented by a single set of mean values for each hour of our predetermined time duration, regardless of the number of bus routes passing through that area. Our analysis and visualization all used 30 m road segments as the unit. This way of generating road segment profiles has extensive details showing spatial and temporal variations in temperature across the city. In addition, it takes a conservative approach and avoids overestimating temperatures in areas without data points, unlike other interpolation methods. Additionally, these 30 m road segments were directly generated along with the Athens Transit and UGA Transit bus routes.

An important aspect of our data reduction approach was the retention of temperature extremes. Although we reduced the amount and limited the dataset's variabilities, we did not filter out 'peak' values as outliers like other environment monitoring projects.[19,31] Peak values may occur due to proximity to other vehicles' exhaust fumes or various human-made heat sources.[32] These values reveal the origin of high AAT and the road network's impact.[18] These values can be challenging to predict and model with limited data collection, but in our study's duration, consistent heat emissions should be reflected in the data and not considered as anomalies. The only outliers removed were extreme low values compared to the weather station records which can occur during vehicle maintenance and preset error signals.

2.3 Spatial–temporal hotspot analysis

With our aggregated dataset prepared, we applied spatial–temporal analytical methods to identify and characterize urban heat patterns. The primary objective of the spatio–temporal analysis is to identify the variability in hotspots across the city by time. We chose hotspot analysis as our primary method and we focus on relative hotspots across the city to allow comparison across days and months without considering the general ambient weather conditions. For example, a temperature of 30 °C might be a hotspot on one day but not on another day or month.

To ensure that our analysis captured heat patterns under diverse weather conditions, we stratified our data based on the ambient temperature regime. Our study covers the summer period, during which daily variations in maximum air temperatures at the local airport weather station can exceed 10 °C. To address our first objective of assessing the consistency of the hottest areas under different ambient conditions, we identified the hottest spots under various temperature regimes, including average days, hot days, and very hot days. We then compared the occurrences of these hottest spots. Each day was classified relative to a threshold based on the daily maximum air temperature recorded at the Ben Epps airport, which is operated by the National Weather Service (NWS) and Federal Aviation Administration (FAA) (SI Appendix, Table S1). July, the hottest month of the year, was included in our study. Since temperature patterns vary seasonally, we applied monthly classification thresholds for the study period (May through September 2019) using 30-year climate normals for Athens, GA.[28] For each month, we categorized days as "normal" when maximum temperatures were near the long-term average (May: 27.2 °C; June: 30.6 °C; July: 32.2 °C; August: 31.7 °C; September: 28.3 °C), "hot" when temperatures were one standard deviation ($\sigma = 3$ °C) above average, and "very hot" when temperatures were two standard deviations ($\sigma = 6$ °C) above average. This classification ensured that the general weather conditions within each group were similar and allowed for averaging without significant loss of variability while accounting for seasonal temperature differences.

Having established our data stratification approach, we now describe the spatial–temporal hotspot analysis methodology.

Hotspot analysis is a spatial analysis and mapping technique that aims to identify clusters of spatial phenomena.[33,34] These spatial phenomena are represented as points on a map and can refer to the locations of events or objects, such as crime incidents or accidents. Additionally, these points can also represent the intensities of events or objects for analyzing continuous landscapes.[35,36] Hotspot analysis can also locate areas with relatively high values, regardless of whether the absolute value is high or low, thus minimizing the impact of diurnal fluctuations in reference weather.

Spatio–temporal hotspot analysis, or emerging hotspot analysis, incorporates a temporal component based on Tobler's first law of geography. In addition to the influence of nearby places, this method recognizes that places at the current time can also affect the upcoming situation. This approach has been widely used in various ecological and project contexts where missing data and temporal information are common issues.[37,38]

Our spatio–temporal hotspot analysis involves several steps. First, we perform spatial pattern analysis with temporal influence from the previous hour. Subsequently, a hotspot map is generated to visualize the heat profile of the study area, showcasing different types of hotspots, such as persistent, consecutive, and oscillating hotspots.[39,40] In this step, road segments are categorized as notable hotspots by being hotter than surrounding areas about 25–50% of the time.

Various spatial analytics techniques are available, including the neighborhood nearest index, Moran's I, Gi* statistics, and others. Moran's I is preferred over the neighborhood nearest index because it accounts for spatial autocorrelation events and avoids index inflation in the Gi* statistic when clusters have a small number of observations,[41] making it essential for our study due to the presence of such clusters. Although Moran's I may encounter challenges in selecting the optimal weight for calculation, this issue is minor when spatial dependency is low.[41,42]

In our study, neighboring temperatures influence air temperature,[43] but the impact is more dependent on local biophysical conditions.[44,45] This means that closer places tend to have similar temperatures but can still exhibit significant variations. Hence, there is no weight selection issue when applying Moran's *I* spatial analysis.

The Moran's *I* autocorrelation formula is:

$$I = \frac{n}{S_0} \frac{\sum_{i=1}^{n} \sum_{j=1}^{n} w_{i,j} z_i z_j}{\sum_{i=1}^{n} z_i^2} \quad (1)$$

where z_i is the deviation of an attribute for feature i from its mean $(x_i - \bar{X})$, $w_{i,j}$ is the spatial weight between feature i and j, n is equal to the total number of features, and S_0 is the aggregate of all the spatial weights:

$$S_0 = \sum_{i=1}^{n} \sum_{j=1}^{n} w_{i,j} \quad (2)$$

The z_I score for the statistics is computed as:

$$z_I = \frac{I - E[I]}{\sqrt{V[I]}} \quad (3)$$

where:

$$E[I] = -1/(n-1) \quad (4)$$

$$V[I] = E[I^2] - E[I]^2 \quad (5)$$

By applying this method, each 30 m LST pixel is assigned a value representing its heat profile for a specific hour during each month or the entire season. The generated hotspot value illustrates the relative heat intensity of a particular location compared to its neighboring areas. We have chosen to utilize relative values rather than absolute values due to the considerable variability in temperature. And the calculated values are capable of indicating the dynamic heat profile of each place along the bus route.

2.4 Spatial–temporal visualization of AAT, LST and analysis data

To effectively communicate the complex spatial–temporal patterns revealed by our analysis, we developed a multi-platform visualization strategy. With a vast amount of data, we employed a variety of imagery to present our results concisely. For visualization purposes, we utilized Python spatial data processing toolboxes along with Kepler.gl. Kepler.gl is a powerful open-source geospatial analysis tool that is built on top of Mapbox graphics libraries.[46] We imported the cleaned AAT data points into Python and utilized the mapping function of Kepler.gl to create our maps. Through coding and the importation of libraries in Python or directly on the webpage, we were able to easily achieve different visualization options, including points, lines, polygons, and hexagons. Furthermore, we could incorporate various visualization functions such as data filtering, dropdown options for color ramp and feature sizes, as well as zoom in and out capabilities, by calling the respective codes and importing the necessary library packages.

As a result, we created hotspot maps at different times of the day and produced a comprehensive set of images and a video illustrating the dynamic variation of daily hotspots throughout the entire city using Kepler.gl. In all our AAT visualizations, we used an aggregation size of 90 meters. We chose this size to ensure better visibility of all pixels within the city, as the 30-meter aggregation size was hardly discernible when plotted on the map.

To enable comparison between ground-level and satellite-based temperature measurements, we plotted the Land Surface Temperature (LST) alongside the generated hotspot analysis results, respectively. The LST data were obtained directly from the Landsat 7/8 analysis ready data published by USGS, which was processed using a mono-band algorithm.[47] The LST flyover time for the study area occurs at 11:30 am or 12:30 pm local time, depending on whether daylight saving time is in effect. This flyover happens every 16 days for both the Landsat 7 and Landsat 8 datasets. In addition to this, other supporting datasets were utilized for comparison and

visualization purposes. These included Google street view image screenshots, city 3D models generated from LiDAR data points of Athens, and the UGA trees dataset. The UGA trees dataset provides information about tree locations, as well as the diameter and height of their canopies. However, for the purpose of providing a general idea of the urban canopy size, we used only the diameter of the canopies as input values. To clearly indicate the locations of tree plantings on the graph, we represented the trees using a standardized size rather than reflecting the specific heights of individual trees.

3. Results

3.1 Visualizing the collected drive-by sensing AAT data

We used Kepler.gl to draw Athens AAT maps every day from May through November 2019. In the figure below, we demonstrated data visualization from September 3rd, 2019, to September 4th, 2019, where daily maximum temperatures are two standard deviations higher than the mean daily max temperature of the September Athens 30-year normal, for the morning (30 minutes before and after 9 am), noon (30 minutes before and after 12 pm), afternoon (30 minutes before and after 3 pm), and early evening (30 minutes before and after 6 pm) (Fig. 1). Each pixel in the images is 90 by 90 meters for the purpose of visualization. From the figures shown below, spatial and temporal variations of hotspots are evident across the city at places with a higher level of urbanization. Places from the highly urbanized places can be more than 12 °C hotter than other places throughout noon to evening of the day. Generally, during a summer day, the highest temperature appears around the early afternoon.

Additionally, many spatial variations across the city were observed in the above images. These spatial variabilities also varied daily which requires hotspot analysis to extract such information.

3.2 Overview of the spatial distribution and magnitude of urban road hotspots

We continued the above visualization and analysis by assigning drive-by-sensed data to road segments for hotspot analysis. In hotspot analysis, we categorized each road segment as a hotspot, coldspot, or neither hot/cold spot and made a categorization for each hour. In the end, we summarized the occurrence and generated a hotspot profile map for all road segments along the bus routes for the 2019 warm season (May–Sep.) (Fig. 2). According to this map, specific road segments around the university campus and near suburban businesses have higher chances of being hotspots, while the city downtown is not a hotspot center (Fig. 2a).

The Landsat map shown above was generated by averaging four images from the 2019 warm season: June 14, July 24, August 17, and September 02. The July 24 image is from Landsat 7, resulting in Scan Line Corrector (SLC) gaps. As for July, no Landsat 8 images were available due to cloud cover. The average was calculated using all four images for locations outside the gaps, while for locations within the gaps, the average was based on the other three images.

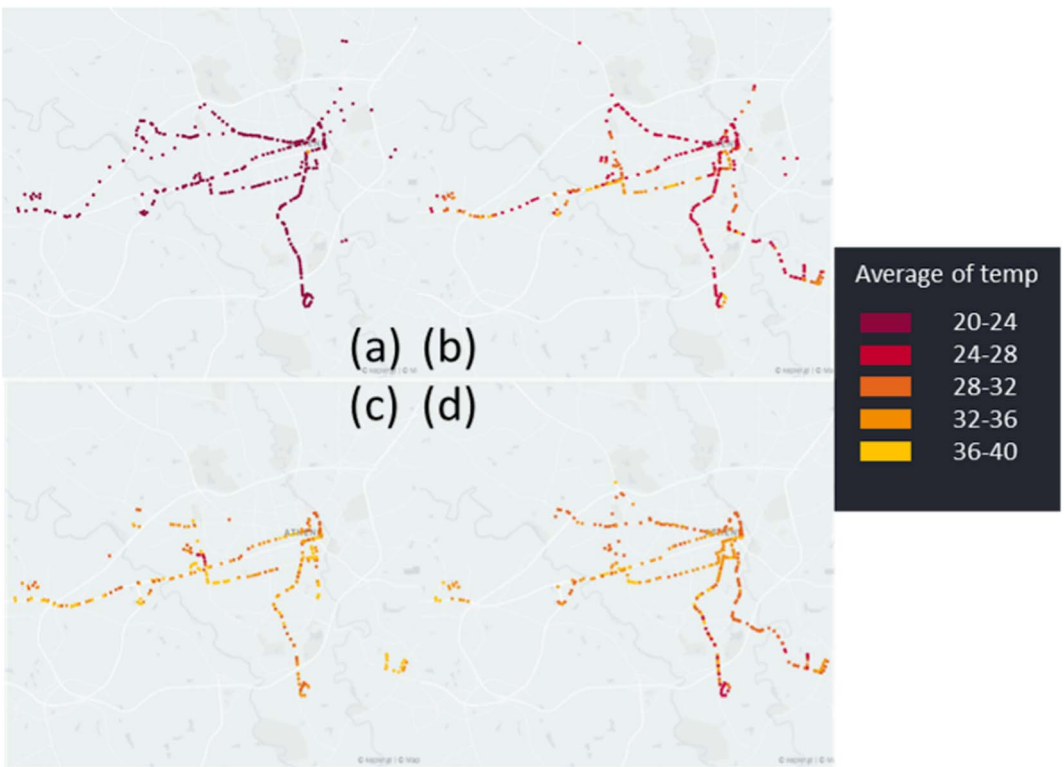

Fig. 1 Temporal AAT map for Sep. 3, 2019, (a) Sep. 3rd morning at 9 am, (b) Sep. 3rd morning at 12 pm, (c) Sep. 3rd afternoon at 3 pm, and (d) Sep. 3rd evening at 6 pm.

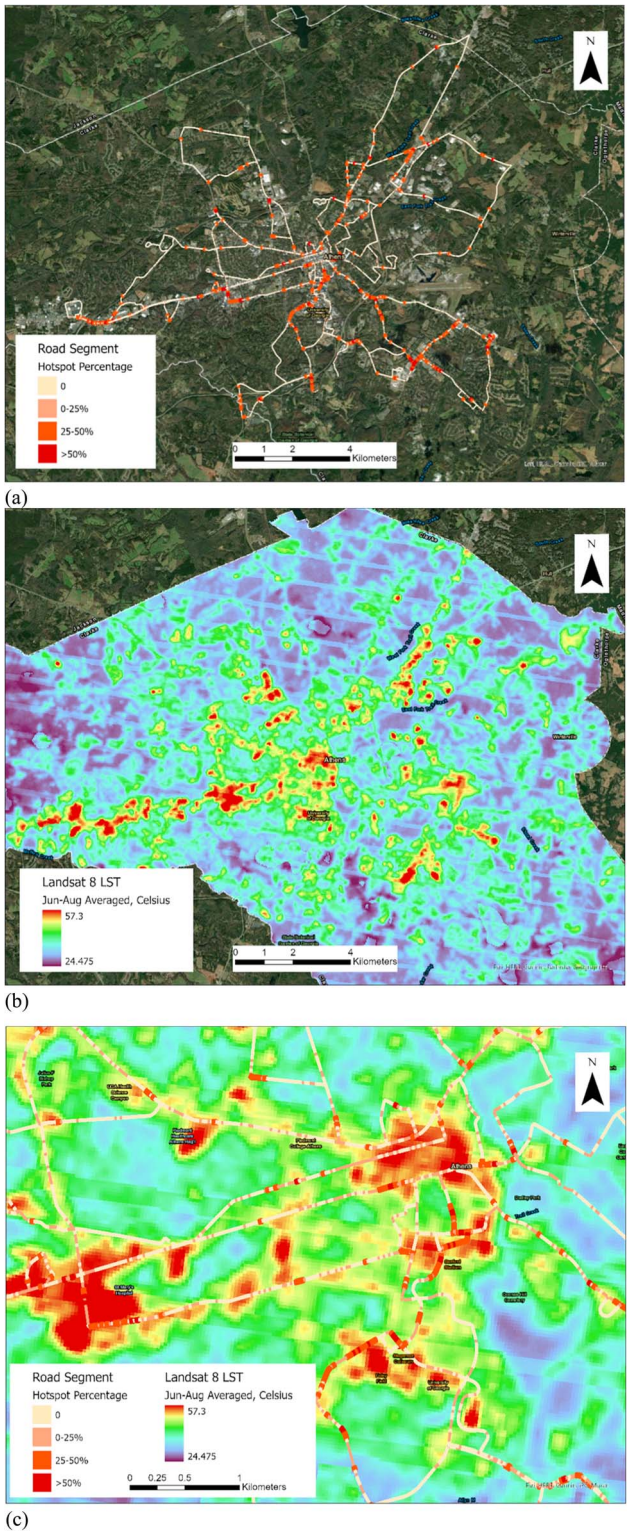

Fig. 2 Maps of (a) chances of each road segment being a hotspot across the daytime during summer 2019, with (b) averaged Landsat LST of Landsat 8 LST from September 2nd, 2019, and (c) zoomed-in hotspot map with LST map of downtown and the university campus.

When comparing the results of hotspot analysis with satellite-derived LST images, we observed that not all hotspots corresponded to high-temperature areas depicted in the LST images (Fig. 2c). Additionally, numerous high-temperature areas displayed in the LST images were not identified as hotspots according to the hotspot analysis results (Fig. 2c), specifically the roads traversing the downtown area. These differences between the two maps indicate that LST provides a general overview of hot places but does not correlate with ground-measured AAT data obtained through drive-by sensing, as LST primarily captures the emittance while our sensors recorded the ambient heat. These disparities will be further explored and elaborated upon in subsequent sections, including detailed comparisons of urbanized regions and adjacent road segments.

We summarize our hotspot analysis findings in Table 1. The result is similar to the Kepler.gl visualization (Fig. 1) in that the temperature differences can be as high as 12 °C between hot and cold spots. About 10% of all the road segments are categorized as notable hotspots by being hotter than surrounding areas about 25–50% of the time. However, only 1% of all road segments can be hot throughout the whole day as persistent hotspots, which suggests a strong temporal variation in the hotspot distribution.

3.3 Hyperlocal temporal thermal profiles of urban built environments

We observed prominent hotspots near a football stadium and various parking lots and several road intersections near shopping plazas around the city. All road segments are homogeneous asphalt roads. These are popular points of interest (POIs) where people tend to congregate and are exposed to extreme heat.[48] Summer noontime LST maps from Landsat indicate that downtown areas are hotspots with the highest surface temperatures (Fig. 2b). However, based on our drive-by-sensed data, these areas were only 2 °C hotter on average during noon compared to the surrounding more vegetated regions (Fig. 1). In contrast, it was observed that many of the aforementioned prominent hot places identified by drive-by sensing do not exhibit extreme LST (Fig. 2c). This observation was made through visual comparison, while a more robust approach would involve using certain statistical methods, such as regression analysis or geostatistical techniques,[49] to extract the heat profile from all these diverse AAT observations and enable an overall match and comparison. This highlights the usefulness and benefits of hotspot analysis, as demonstrated by the examples provided below. And additional spatial variability of the heat profile can be directly visualized from the analysis result.

The campus near the football stadium and parking lots has relatively higher temperatures, mostly during noon and afternoon (bottom left part of Fig. 3a). These road sections are hotspots regardless of whether it is an average, hot, or very hot day as defined by weather station data. Consistent with previous studies,[50,51] the impervious surfaces and lack of green space at these locations significantly increase the ambient temperature by 4–8 °C (Fig. 3a). Also, these places are not surrounded by high buildings which reduce shading-induced coldspots. In contrast, the top left road segments on the west side of the high-traffic

Table 1 Hotspot analysis results summarized by number of segments for different times of a day and average magnitude of the hot–cold spot difference

Number of segments	Total segments	50% or more hotter	25–50% hotter	Hot–cold magnitude (°C)
For all types of day	6005	52	342	9
Morning	6005	12	28	9
Noon	6005	40	529	11
Afternoon	6005	59	588	12
Cold spot	6005	23	227	—
For normal days	6005	32	234	8
For hot days	6005	38	209	8
For very hot days	6005	32	234	9

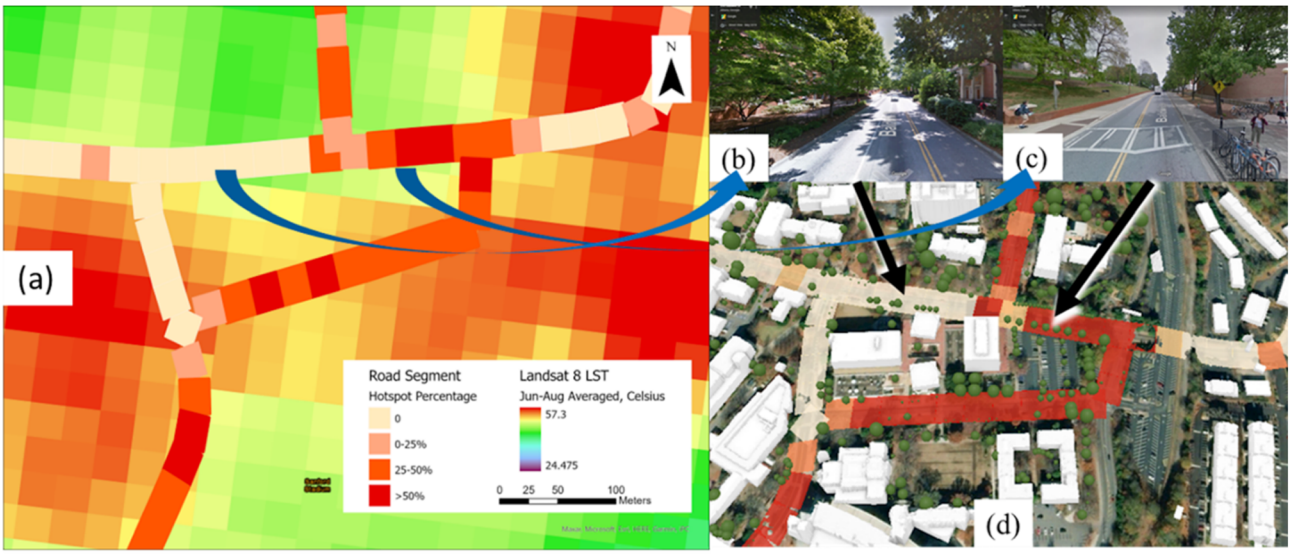

Fig. 3 Google street view and 3D model of the canopy cover of west and east of the crossing, (a) LST with hotspot profile, google street view of (b) west and (c) east of the crossing, and (d) hotspot and 3D model of the crossing.

streets are well-shaded by trees (Fig. 3). Trees were present next to the road on the west side of the crossing (Fig. 3b and d), while the sidewalk is between the trees and the east side (Fig. 3c and d). Additionally, these west-east oriented roads, showed up as hotspots during the morning potentially due to their orientation aligning with the sun azimuth.

This phenomenon also contributes to the fact that downtown is not a prominent hotspot. Areas around downtown and shopping plazas in the city have many impervious surfaces and buildings nearby (SI Appendix, Fig. S2). However, downtown areas have trees and buildings next to the roads, creating shade to cool off the ambient temperatures (SI Appendix, Fig. S2a, and S2c). Therefore, commonly used LST data in urban heat analysis studies from satellite images have limited capability of representing localized heat distribution and hotspot dynamics. And our approach can better capture the hyperlocal conditions than remotely sensed data.

3.4 Heat exposure dynamics related urban thermal hotspot profile

In our hotspot analysis, we found several areas with elevated ambient temperatures that corresponded to well-visited locations. As shown in Fig. 4a, several commonly visited POIs (*e.g.* l grocery stores, hospitals, schools, and libraries) are in close proximity and are located on hotter road segments. Common high-traffic areas such as complexes comprising retailers, restaurants, and cinemas had elevated temperatures and were in proximity to these hotspots. Similar elevated temperatures were observed across the city near an athletic complex which is also commonly visited by children and adolescents. The complex hosts outdoor activities which are another "hot" area with little shade provided by structures or trees for athletes or spectators (SI Appendix, Fig. S3). Hotspot values for the roads around this area are already high, so this area may be designated as one of the vulnerable locations for implementing heat mitigation engineering. Our hyperlocal analysis helps identify and prioritize hotspots within the city, which are often missed by satellite-scale analysis.

In addition to the increased heat exposure near some POIs, our review of thermal exposure and bus stops provides another example of how these data can be used to address heat hazards to specific constituencies. The hotspot profile of each bus stop across the city was determined (Fig. 4b) and it was observed that bus stops have a relatively higher chance of being located near

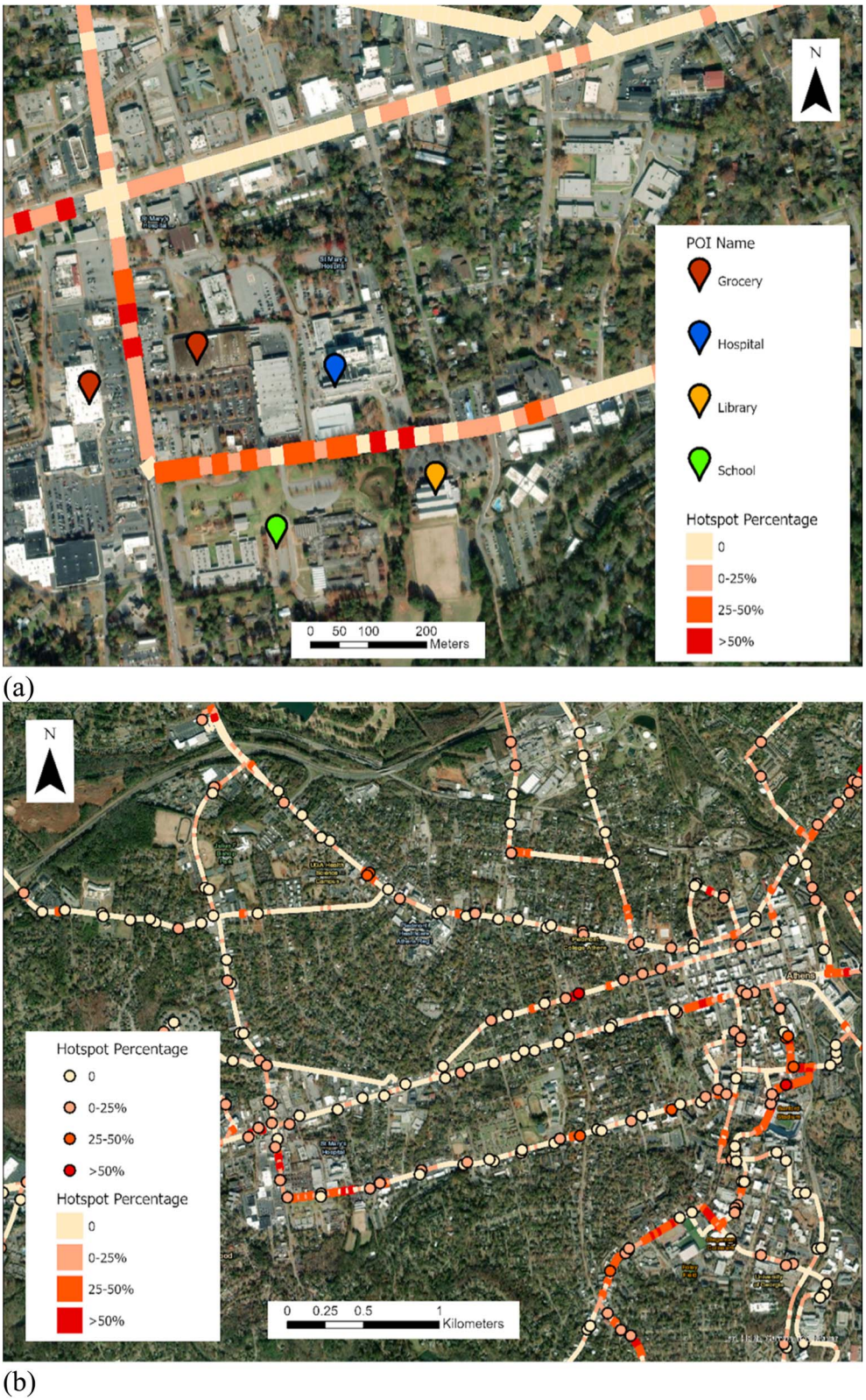

Fig. 4 Hotspot map near public facilities around the city (a) featuring hospitals, grocery, libraries, and schools, (b) with bus stops highlighted.

hotspots than general road segments (SI Appendix, Fig. S4). Out of all 539 bus stops within the city, 281 bus stops are within the hotspot road segments, while for all 6005 road segments, less than 1/3 (1775) road segments can be hotspots.

Google street views of pairs of hot and non-hotspots also indicated a great need for corresponding heat mitigation plans for bus stops (SI Appendix, Fig. S5). A well canopy-covered bus stop can be a non-hotspot anytime during the study period,

while another bus stop without shade can be a hot spot for 25% of the time, thus indicating the capability of our approach for targeting certain locations for heat mitigation.

4. Discussion

This study presented the hyperlocal variability of urban heat at any given time in a mid-sized city and also highlighted the advantages of using emerging sensing technologies to obtain such high-frequency environmental parameters. Drive-by sensing using public transport buses provides an excellent resource for data collection. These vehicles routinely operate for long periods of the day across large portions of the city, where people live, go to school, seek entertainment, and work. These spatial and temporal resolutions of the drive-by-sensing data allow for detailed analysis of how heat might affect certain groups, such as bus riders waiting at bus stops. Such vehicle-borne sensing platforms and techniques can be replicated and scaled to different sized cites.

We generated rich details of the 30 m city's thermal landscape *via* the collected AAT data and extensive hotspot analysis with different visualization techniques. LST, traditionally used in urban heat island studies, does not always correspond to AAT.[52,53] It has been widely acknowledged that LST tends to be higher than AAT, and that LST is more strongly influenced by horizontal surfaces than vertical ones.[54] Studies resort to using LST when AAT data are unavailable. In this study, we collected AAT data to demonstrate the extent of variations between the two measures. Our analysis shows that AAT from mobile sensors is a better indicator for dynamic heat exposure over space and time than satellite LST products or weather station temperature data. For human thermal exposure studies, it is more appropriate to use AAT. It is crucial to recognize the significant mismatch between LST and AAT. Although not directly shown in this study, many highly urbanized places have LST over 50 °C as shown in Fig. 2b while the highest temperature was less than 40 °C (shown in Fig. 1). Relying solely on LST for urban planning and other decision-making processes can result in misleading mitigation strategies.

Our approach allowed us to look at the dynamic spatial–temporal variations of hotspots within our study area. The hotspots are primarily around more urbanized land cover locations with impervious surfaces, which supports previous work.[50,55] Downtown was not the hottest location in this midsize city because of the shade from buildings and trees as opposed to results from Ghribi and Dahech[56] who found downtown Sfax in Tunisia to be consistently 2 °C hotter than other urban areas. But our results were consistent with several previous studies based on fine scale measurement.[57,58] In addition, we observed that hotspots were not static and varied over time. Certain areas were the hottest during noon and afternoon (*e.g.*, stadiums), and others, such as west-east oriented roads, showed up as hotspots during the morning due to their orientation aligning with the sun angle (Fig. 3). Importantly, we found that there isn't always a single city hotspot, unlike what less resolved datasets may suggest.

The multicentric hotspots present across the city suggest that simplistic approaches to heat mitigation as guided by low-resolution data sources may not be effective. Our study highlights how knowledge of the hyperlocal thermal profile can guide city planners to target hot locations more efficiently and effectively with mitigation measures such as adding water bodies, cooling stations, green space, and shading infrastructure.[11,59] In addition, the hyperlocal data can be blended with information on POIs or locations with known vulnerable populations to guide interventions to make the community more sustainable.[60–62]

A unique aspect of our work is that it integrates the Internet of Things (IoT) enabled drive-by sensing with virtual representation and visualization frameworks such as Kepler.gl, Google street view, and 3D city modeling. This innovative combination offers two distinct benefits. First, it will enable scientists, city planners, and community managers (*e.g.*, county officials) to intuitively understand the heat vulnerability characteristics of their cities at a fine granularity (*e.g.*, block-level) and analyze the effects of geographical artifacts such as buildings and vegetation on thermal characteristics of the city.[63] Second, it will also enable city residents to get a sense of the impact of their daily activities, such as running, outdoor work, *etc.*, on their individual heat exposure, thereby helping them to reduce their heat exposure risks and alleviate heat vulnerabilities in urban communities. In the future, we can develop a tool for running or navigation apps that blend the map with our temperature data along the road to suggest cooler paths over hot paths.

We recognize, of course, that drive-by sensing has some limitations. Most importantly, it gathers data on certain roads traversed by public transportation and misses areas not planned or accessible to these vehicles. Yet, public transportation provides an ideal foundation for monitoring temperatures with regular routes and patterns across populated areas.[25] Additionally, many points of interest like shops and offices are in close proximity to roads. Other fleets of vehicles such as sanitation trucks or other service vehicles would increase the sampling network. Also,[18] reported a blended product that would leverage the strength of drive-by-sensing with other sources of data to provide broader coverage at high spatial and temporal resolutions using machine learning techniques. Finally, our AAT measurements are collected closer to the surface than *in situ* AAT measurements. We feel that our values are still comparable to AAT measurements at anthropomorphic heights because the turbulent mixing caused by the moving buses would reduce the environmental lapse rate and temperature differences over those short differences in height.[29]

In conclusion, we show that vehicle-borne sensing is an important emerging technology that can be effectively coupled with other data-gathering sources. This innovative approach enhances our understanding of human thermal exposures by providing high-resolution, spatially diverse temperature data, ultimately leading to more informed public health strategies and urban planning initiatives. While tested in a medium-sized city, our methodology is easily scalable to larger urban areas, especially those with robust public transportation systems. This

will improve our understanding of urban heat dynamics for mitigating heat hazards in making cities more sustainable.

Author contributions

Yanzhe Yin: conceptualization, data curation, software, formal analysis, visualization, writing – original draft. Andrew Grundstein: conceptualization, methodology, investigation, writing-review and editing. Deepak R. Mishra: conceptualization, methodology, funding acquisition, project administration, writing- review and editing. Navid Hashemi Tonekaboni: data curation, software, visualization, validation. Lakshmish Ramaswamy: conceptualization, methodology, writing- review and editing. John A. Miller: methodology. John Dowd: data curation, software.

Conflicts of interest

There are no conflicts of interest to declare.

Data availability

The data that support the findings of this study are available on request from the corresponding author Y. Y. As there are manuscripts describing the dataset pending to be published, the data are only available per request.

Supplementary information (SI) is available. See DOI: https://doi.org/10.1039/d5va00332f.

Acknowledgements

This research was funded by the (NSF) S&CC: Smart & Connected Communities program (Grant # 1637277). We would like to thank the University of Georgia's (UGA) Transportation Services and Athens-Clarke County (ACC) Unified Government's Transit Department for allowing us to mount the sensors on their buses and answer numerous questions throughout the projects. Special Thanks to Butch McDuffie, Director ACC Transit, and Don Walter, Director UGA Transit, for their support.

References

1 J. Dong, J. Peng, X. He, J. Corcoran, S. Qiu and X. Wang, Heatwave-induced human health risk assessment in megacities based on heat stress-social vulnerability-human exposure framework, *Landsc. Urban Plann.*, 2020, **203**, 103907.

2 K. L. Ebi, A. Capon, P. Berry, C. Broderick, R. de Dear, G. Havenith, Y. Honda, R. S. Kovats, W. Ma, A. Malik, N. B. Morris, L. Nybo, S. I. Seneviratne, J. Vanos and O. Jay, Hot weather and heat extremes: health risks, *Lancet*, 2021, **398**, 698–708.

3 C. Tuholske, K. Caylor, C. Funk, A. Verdin, S. Sweeney, K. Grace, P. Peterson and T. Evans, Global urban population exposure to extreme heat, *Proc. Natl. Acad. Sci. U. S. A.*, 2021, **118**, e2024792118.

4 G. A. Meehl and C. Tebaldi, More intense, more frequent, and longer lasting heat waves in the 21st century, *Science*, 2004, **305**, 994–997.

5 V. Mishra, A. R. Ganguly, B. Nijssen and D. P. Lettenmaier, Changes in observed climate extremes in global urban areas, *Environ. Res. Lett.*, 2015, **10**, 024005.

6 J. Kennedy, *WMO Provisional State of the Global Climate 2022*, <bound method Organization.get_name_with_acronym of <Organization: World Meteorological Organisation>>, 2022.

7 A. M. Vicedo-Cabrera, N. Scovronick, F. Sera, D. Royé, R. Schneider, A. Tobias, C. Astrom, Y. Guo, Y. Honda, D. M. Hondula, R. Abrutzky, S. Tong, M. de S. Z. S. Coelho, P. H. N. Saldiva, E. Lavigne, P. M. Correa, N. V. Ortega, H. Kan, S. Osorio, J. Kyselý, A. Urban, H. Orru, E. Indermitte, J. J. K. Jaakkola, N. Ryti, M. Pascal, A. Schneider, K. Katsouyanni, E. Samoli, F. Mayvaneh, A. Entezari, P. Goodman, A. Zeka, P. Michelozzi, F. de'Donato, M. Hashizume, B. Alahmad, M. H. Diaz, C. D. L. C. Valencia, A. Overcenco, D. Houthuijs, C. Ameling, S. Rao, F. Di Ruscio, G. Carrasco-Escobar, X. Seposo, S. Silva, J. Madureira, I. H. Holobaca, S. Fratianni, F. Acquaotta, H. Kim, W. Lee, C. Iniguez, B. Forsberg, M. S. Ragettli, Y. L. L. Guo, B. Y. Chen, S. Li, B. Armstrong, A. Aleman, A. Zanobetti, J. Schwartz, T. N. Dang, D. V. Dung, N. Gillett, A. Haines, M. Mengel, V. Huber and A. Gasparrini, The burden of heat-related mortality attributable to recent human-induced climate change, *Nat. Clim. Change*, 2021, (11), 492–500.

8 D. Habeeb, J. Vargo and B. Stone, Rising heat wave trends in large US cities, *Nat. Hazards*, 2015, **76**, 1651–1665.

9 H. O. Pörtner, D. C. Roberts, H. Adams, C. Adler, P. Aldunce, E. Ali, R. A. Begum, R. Betts, R. B. Kerr, R. Biesbroek, J. Birkmann, K. Bowen, E. Castellanos, G. Cissé, A. Constable, W. Cramer, D. Dodman, S. H. Eriksen, A. Fischlin, M. Garschagen, B. Glavovic, E. Gilmore, M. Haasnoot, S. Harper, T. Hasegawa, B. Hayward, Y. Hirabayashi, M. Howden, K. Kalaba, W. Kiessling, R. Lasco, J. Lawrence, M. F. Lemos, R. Lempert, D. Ley, T. Lissner, S. Lluch-Cota, S. Loeschke, S. Lucatello, Y. Luo, B. Mackey, S. Maharaj, C. Mendez, K. Mintenbeck, M. M. Vale, M. D. Morecroft, A. Mukherji, M. Mycoo, T. Mustonen, J. Nalau, A. Okem, J. P. Ometto, C. Parmesan, M. Pelling, P. Pinho, E. Poloczanska, M.-F. Racault, D. Reckien, J. Pereira, A. Revi, S. Rose, R. Sanchez-Rodriguez, E. L. F. Schipper, D. Schmidt, D. Schoeman, R. Shaw, C. Singh, W. Solecki, L. Stringer, A. Thomas, E. Totin, C. Trisos, D. Viner, M. van Aalst, M. Wairiu, R. Warren, P. Yanda and Z. Z. Ibrahim, Climate change 2022: impacts, adaptation and vulnerability, *Uniwersytet śląski*, 2022, **7**, 343–354.

10 O. Jay, A. Capon, P. Berry, C. Broderick, R. de Dear, G. Havenith, Y. Honda, R. S. Kovats, W. Ma, A. Malik, N. B. Morris, L. Nybo, S. I. Seneviratne, J. Vanos and K. L. Ebi, Reducing the health effects of hot weather and heat extremes: from personal cooling strategies to green cities, *Lancet*, 2021, **398**, 709–724.

11 K. R. Gunawardena, M. J. Wells and T. Kershaw, Utilising green and bluespace to mitigate urban heat island intensity, *Sci. Total Environ.*, 2017, **584–585**, 1040–1055.
12 J. Qi, L. Ding and S. Lim, Application of a decision-making framework for multi-objective optimisation of urban heat mitigation strategies, *Urban Clim.*, 2023, **47**, 101372.
13 B. A. Norton, A. M. Coutts, S. J. Livesley, R. J. Harris, A. M. Hunter and N. S. G. Williams, Planning for cooler cities: A framework to prioritise green infrastructure to mitigate high temperatures in urban landscapes, *Landsc. Urban Plann.*, 2015, **134**, 127–138.
14 P. A. Mirzaei, Recent challenges in modeling of urban heat island, *Sustain. Cities Soc.*, 2015, **19**, 200–206.
15 J. A. Voogt and T. R. Oke, Thermal remote sensing of urban climates, *Remote Sens. Environ.*, 2003, **86**, 370–384.
16 Q. Weng, Fractal analysis of satellite-detected urban heat island effect, *Photogramm. Eng. Remote Sens.*, 2003, **69**, 555–566.
17 Q. Weng and P. Fu, Modeling annual parameters of clear-sky land surface temperature variations and evaluating the impact of cloud cover using time series of Landsat TIR data, *Remote Sens. Environ.*, 2014, **140**, 267–278.
18 Y. Yin, N. H. Tonekaboni, A. Grundstein, D. R. Mishra, L. Ramaswamy and J. Dowd, Urban ambient air temperature estimation using hyperlocal data from smart vehicle-borne sensors, *Comput. Environ. Urban Syst.*, 2020, **84**, 101538.
19 R. Kotharkar and A. Bagade, Evaluating urban heat island in the critical local climate zones of an Indian city, *Landsc. Urban Plann.*, 2018, **169**, 92–104.
20 Q. Zhao and E. Wentz, A MODIS/ASTER Airborne Simulator (MASTER) Imagery for Urban Heat Island Research, *Data*, 2016, **1**, 7.
21 H. C. Ho, A. Knudby, Y. Xu, M. Hodul and M. Aminipouri, A comparison of urban heat islands mapped using skin temperature, air temperature, and apparent temperature (Humidex), for the greater Vancouver area, *Sci. Total Environ.*, 2016, **544**, 929–938.
22 I. Kloog, A. Chudnovsky, P. Koutrakis and J. Schwartz, Temporal and spatial assessments of minimum air temperature using satellite surface temperature measurements in Massachusetts, USA, *Sci. Total Environ.*, 2012, **432**, 85–92.
23 B. Stone, J. Vargo, P. Liu, D. Habeeb, A. DeLucia, M. Trail, Y. Hu and A. Russell, Avoided Heat-Related Mortality through Climate Adaptation Strategies in Three US Cities, *PLoS One*, 2014, **9**, e100852.
24 E. Mallen, J. Bakin, B. Stone, R. Sivakumar and K. Lanza, Thermal impacts of built and vegetated environments on local microclimates in an Urban University campus, *Urban Clim.*, 2020, **32**, 100640.
25 A. Anjomshoaa, F. Duarte, D. Rennings, T. J. Matarazzo, P. Desouza, C. Ratti, A. Anjomshoaa, C. Ratti, F. Duarte and P. Desouza, City Scanner: Building and Scheduling a Mobile Sensing Platform for Smart City Services, *IEEE Internet Things J.*, 2018, **5**, 4567–4579.
26 J. Voelkel and V. Shandas, Towards Systematic Prediction of Urban Heat Islands: Grounding Measurements, Assessing Modeling Techniques, *Climate*, 2017, **5**, 41.
27 C. A. Antonopoulos, T. L. Gilbride, E. R. Margiotta and C. E. Kaltreider, *Guide to Determining Climate Zone by County: Building America and IECC 2021 Updates*, 2022, DOI: 10.2172/1893981.
28 A. Arguez, I. Durre, S. Applequist, M. Squires, R. Vose, X. Yin and R. Bilotta, *NOAA's US Climate Normals (1981–2010)*, NOAA National Centers for Environmental Information, 2010, vol. 10, p. V5PN93JP.
29 S. P. Arya, *Introduction to Micrometeorology*, Academic Press, New York, 2001.
30 N. H. Tonekaboni, S. Kulkarni and L. Ramaswamy, Edge-Based Anomalous Sensor Placement Detection for Participatory Sensing of Urban Heat Islands, *2018 IEEE International Smart Cities Conference*, ISC2, 2018, DOI: 10.1109/ISC2.2018.8656705.
31 L. Zhao, X. Lee, R. B. Smith and K. Oleson, Strong contributions of local background climate to urban heat islands, *Nature*, 2014, (511), 216–219.
32 I. Batur, S. A. Markolf, M. V. Chester, A. Middel, D. Hondula and J. Vanos, Street-level heat and air pollution exposure informed by mobile sensing, *Transp. Res., Part D Transp. Environ.*, 2022, **113**, 103535.
33 E. G. G. T. Luc Anselin, *Crime Mapping and Hot Spot Analysis*, edn. 1st edn., 2008.
34 A. T. Murray, *Detecting Hot Spots Using Cluster Analysis and GIS*, 2001.
35 Y. Jamei, P. Rajagopalan and Q. Chayn) Sun, Spatial structure of surface urban heat island and its relationship with vegetation and built-up areas in Melbourne, Australia, *Sci. Total Environ.*, 2019, **659**, 1335–1351.
36 J. Bruns and V. Simko, Stable Hotspot Analysis for Intra-Urban Heat Islands, *GI_Forum*, 2017, **1**, 79–92.
37 E. L. Betty, B. Bollard, S. Murphy, M. Ogle, H. Hendriks, M. B. Orams and K. A. Stockin, Using emerging hot spot analysis of stranding records to inform conservation management of a data-poor cetacean species, *Biodivers. Conserv.*, 2020, **29**, 643–665.
38 B. Xu, B. Qi, K. Ji, Z. Liu, L. Deng and L. Jiang, Emerging hot spot analysis and the spatial–temporal trends of NDVI in the Jing River Basin of China, *Environ. Earth Sci.*, 2022, **81**, 1–15.
39 S. Chainey, L. Tompson and S. Uhlig, The Utility of Hotspot Mapping for Predicting Spatial Patterns of Crime, *Secur. J.*, 2008, (21), 4–28.
40 S. Anno, T. Hara, H. Kai, M. A. Lee, Y. Chang, K. Oyoshi, Y. Mizukami and T. Tadono, Spatiotemporal dengue fever hotspots associated with climatic factors in Taiwan including outbreak predictions based on machine-learning, *Geospat. Health*, 2019, **14**, 183–194.
41 L. Anselin, Local Indicators of Spatial Association—LISA, *Geogr. Anal.*, 1995, **27**, 93–115.
42 J. K. Ord and A. Getis, Local Spatial Autocorrelation Statistics: Distributional Issues and an Application, *Geogr. Anal.*, 1995, **27**, 286–306.

43 Y. Qian, W. Zhou, X. Hu and F. Fu, The Heterogeneity of Air Temperature in Urban Residential Neighborhoods and Its Relationship with the Surrounding Greenspace, *Remote Sens.*, 2018, (10), 965.
44 N. H. Tonekaboni, A. Grundstein, L. Ramaswamy, S. Kulkarni, D. Mishra and Y. Yin, in *Proceedings of the 1st ACM SIGSPATIAL International Workshop on Advances in Resilient and Intelligent Cities*, ARIC 2018, 2018.
45 Y. Yin, A. Grundstein, D. R. Mishra and N. Hashemi Tonekaboni, *Community-centric Individual Level Approach for Analyzing and Mitigating Urban Heat Hazards*, American Geophysical Union, Fall Meeting, 2018.
46 J. Xia, Q. Huang, Z. Gui and W. Tu, Web-Based Mapping and Visualization Packages, *Open GIS*, 2024, 283–314.
47 J. L. Dwyer, D. P. Roy, B. Sauer, C. B. Jenkerson, H. K. Zhang and L. Lymburner, Analysis ready data: Enabling analysis of the landsat archive, *Remote Sens.*, 2018, **10**(9), 1363.
48 Y. Yin, A. Grundstein, D. R. Mishra, L. Ramaswamy, N. Hashemi Tonekaboni and J. Dowd, DTEx: A dynamic urban thermal exposure index based on human mobility patterns, *Environ. Int.*, 2021, **155**, 106573.
49 Q. Meng, Z. Liu and B. E. Borders, Assessment of regression kriging for spatial interpolation – comparisons of seven GIS interpolation methods, *Cartogr. Geogr. Inf. Sci.*, 2013, **40**, 28–39.
50 L. Liu and Y. Zhang, Urban Heat Island Analysis Using the Landsat TM Data and ASTER Data: A Case Study in Hong Kong, *Remote Sens.*, 2011, **3**, 1535–1552.
51 A. Grundstein, Y. Yin, N. Hashemi, D. Mishra, L. Ramaswamy and J. Dowd, Utilizing Low-Cost Temperature Sensors for Analyzing and Mitigating Urban Heat Hazards, AMS, 2019, preprint, https://ams.confex.com/ams/2019Annual/meetingapp.cgi/Paper/352475.
52 E. J. Good, D. J. Ghent, C. E. Bulgin and J. J. Remedios, A spatiotemporal analysis of the relationship between near-surface air temperature and satellite land surface temperatures using 17 years of data from the ATSR series, *J. Geophys. Res.:Atmos.*, 2017, **122**, 9185–9210.
53 L. Sheng, X. Tang, H. You, Q. Gu and H. Hu, Comparison of the urban heat island intensity quantified by using air temperature and Landsat land surface temperature in Hangzhou, China, *Ecol. Indic.*, 2017, **72**, 738–746.
54 S. Khandelwal, R. Goyal, N. Kaul and A. Mathew, Assessment of land surface temperature variation due to change in elevation of area surrounding Jaipur, India, *Egypt. J. Remote Sens. Space Sci.*, 2018, **21**, 87–94.
55 F. Kong, H. Yin, P. James, L. R. Hutyra and H. S. He, Effects of spatial pattern of greenspace on urban cooling in a large metropolitan area of eastern China, *Landsc. Urban Plann.*, 2014, **128**, 35–47.
56 M. Ghribi and S. Dahech, The Impact of the Urban Heat Island on the Sensation of Thermal Comfort and Electricity Consumption in Sfax in Central-Eastern Tunisia during the Hot Season, *Energies*, 2023, **16**, 911.
57 I. Buo, V. Sagris, J. Jaagus and A. Middel, High-resolution thermal exposure and shade maps for cool corridor planning, *Sustain. Cities Soc.*, 2023, **93**, 104499.
58 D. Milošević, A. Middel, S. Savić, J. Dunjić, K. Lau and R. Stojsavljević, Mask wearing behavior in hot urban spaces of Novi Sad during the COVID-19 pandemic, *Sci. Total Environ.*, 2022, **815**, 152782.
59 E. J. Gago, J. Roldan, R. Pacheco-Torres and J. Ordóñez, The city and urban heat islands: A review of strategies to mitigate adverse effects, *Renew. Sustain. Energy Rev.*, 2013, **25**, 749–758.
60 C. O'Malley, P. Piroozfar, E. R. P. Farr and F. Pomponi, Urban Heat Island (UHI) mitigating strategies: A case-based comparative analysis, *Sustain. Cities Soc.*, 2015, **19**, 222–235.
61 C. Smith and G. Levermore, Designing urban spaces and buildings to improve sustainability and quality of life in a warmer world, *Energy Policy*, 2008, **36**, 4558–4562.
62 J. Flocks, F. Escobedo, J. Wade, S. Varela and C. Wald, *Environmental Justice Implications of Urban Tree Cover in Miami-Dade County*, Florida, 2011, vol. 4, pp. 125–134, https://home.liebertpub.com/env.
63 H. Wu, Z. He and J. Gong, A virtual globe-based 3D visualization and interactive framework for public participation in urban planning processes, *Comput. Environ. Urban Syst.*, 2010, **34**, 291–298.

